• Basic Research •

Intermittent fasting ameliorates diabetes-induced meibomian gland dysfunction in mice

Wen-Hui Wang[1], *Han-You Wu*[1], *Jian-Wen Xue*[1], *Xiao-Bing Qian*[1], *Jing Li*[1], *Xing-Yan Lin*[1], *Bo-Yu Yang*[1], *Wei Wang*[2,3], *Ling-Yi Liang*[1]

[1]State Key Laboratory of Ophthalmology, Zhongshan Ophthalmic Center, Sun Yat-sen University, Guangdong Provincial Key Laboratory of Ophthalmology and Visual Science, Guangzhou 510060, Guangdong Province, China
[2]Department of Endocrinology, Sun Yat-sen Memorial Hospital, Sun Yat-sen University, Guangzhou 510120, Guangdong Province, China
[3]Department of Endocrinology, Shenshan Medical Center, Sun Yat-sen Memorial Hospital, Sun Yat-sen University, Shanwei 516600, Guangdong Province, China
Co-first Authors: Wen-Hui Wang and Han-You Wu
Correspondence to: Ling-Yi Liang. Zhongshan Ophthalmic Center, State Key Laboratory of Ophthalmology, 7 Jinsui Road, Guangzhou 510060, Guangdong Province, China. lianglingyi@gzzoc.com; Wei Wang. Sun Yat-sen Memorial Hospital, Sun Yat-sen University, 107 Yanjiang West Road, Guangzhou 510120, Guangdong Province, China. wangw253@mail.sysu.edu.cn
Received: 2025-09-16 Accepted: 2026-02-10

Abstract

● **AIM:** To investigate the effect of intermittent fasting (IF) on diabetes-induced meibomian gland dysfunction (MGD) in a mice model.

● **METHODS:** The diabetic mice underwent an 8-week dietary intervention of *ad libitum* (AL) and IF diet. Meibomian gland (MG) proliferative potential, apoptosis, and ductal hyperkeratinization were assessed using immunofluorescence. Gene expression levels were evaluated by Western blot. Lipid accumulation was observed *via* LipidTox staining. Transmission electron microscopy (TEM) examined intracellular lipids and mitochondrial ultrastructure in acinar cells. Lipidomic and transcriptomic analyses compared MG gene expression and lipid profiles between groups.

● **RESULTS:** IF ameliorated diabetes-induced MGD. IF significantly improved diabetic MG proliferation, apoptosis and lipid metabolism imbalance, as well as improved the expression of the genes involved in lipid metabolism. Simultaneously, the results of lipidomics indicated that IF can effectively modify the types and content of lipids, especially ceramides and cholesterol esters. Transcriptomic results suggested that IF effectively ameliorated cell death and modulated ion channels signaling. IF could ameliorate cell death which might be mediated by the calcium ion signaling pathway to mitigate diabetes-induced MGD.

● **CONCLUSION:** These results provide direct evidence for the feasibility of dietary intervention to improve diabetes-induced MGD. IF can alter MG lipid composition and inhibit apoptosis in diabetic condition. The underlying mechanism may be associated with calcium ion signaling pathway.

● **KEYWORDS:** intermittent fasting; meibomian gland dysfunction; diabetic mice; calcium signaling

DOI:10.18240/ijo.2026.05.02

Citation: Wang WH, Wu HY, Xue JW, Qian XB, Li J, Lin XY, Yang BY, Wang W, Liang LY. Intermittent fasting ameliorates diabetes-induced meibomian gland dysfunction in mice. *Int J Ophthalmol* 2026;19(5):846-857

INTRODUCTION

The meibomian gland (MG), a special kind of modified sebaceous gland, comprises ducts and tufted adipogenic acini arranged in parallel within the tarsal plate of both the upper and lower eyelids[1]. The quality and quantity of meibum lipids are essential for ocular surface, as they play a critical role in stabilizing the tear film on the ocular surface. These lipids form a superficial layer that minimize evaporation, prevent dehydration, and establish a protective barrier against microorganisms on the ocular surface[2].

Various conditions, notably those involving high-fat diet, can substantially affect this tissue and set off a series of pathophysiological changes, which can lead to MG dysfunction (MGD)[3]. MGD is characterized by obstruction of the MG terminal ducts, acinar cell loss, and qualitative and quantitative alterations in meibum secretion[4-6]. This impairment interferes with the equilibrium of the ocular surface micro-environment, resulting in unstable tear film, greater tear evaporation, and increased osmolarity, which subsequently triggers persistent inflammatory cascades[7-8].

Diabetes is a prevalent chronic metabolic disorder, with its incidence having risen over the years[9]. A growing body of evidence indicates that diabetes serves as a significant risk factor for the development of MGD[10-11]. Diabetic MGs exhibit numerous morphological and cytological alterations in their acinar and ductal structures[12], and MGD tends to be more severe in diabetic patients[10]. Researches have demonstrated that elevated glucose levels exerted a toxic effect on immortalized human MG epithelial cells[13].

Dietary intervention has been regarded as an important part of diabetes management. Caloric restriction and intermittent fasting (IF) are recognized as nonpharmacological approaches for the prevention and treatment of conditions such as diabetes, obesity, and aging. Nevertheless, caloric restriction may result in nutrient deficiencies, fatigue[14], a reduced metabolic rate, and an elevated risk of subsequent obesity[15], infertility[14], and immune suppression[16]. In contrast, IF mitigates the adverse effects associated with caloric restriction by limiting food intake to specific times of the day or certain days of the week. IF is a health management approach that adjusts eating patterns by alternating between “eating windows” and “fasting windows”. Common methods include the 16:8 method, 5:2 method, and 24-hour fasting, among others. The 24-hour fasting is one of the more commonly used IF methods[17-18]. Consequently, IF may offer a more advantageous strategy compared to chronic caloric restriction, as it integrates the beneficial physiological effects of fasting with a recovery period during the feeding phase, which facilitates regeneration and promotes tissue repair[19]. However, its impact on diabetes-related ocular complications and MGD remains inadequately understood.

This study seeks to undertake a preliminary investigation into the effects of dietary intervention patterns on MGD in diabetic mice, with the objective of elucidating the influence of dietary patterns on hyperglycemia-induced MGD. The findings may offer novel insights into the diagnosis and treatment of diabetic complications, as well as contribute to the dietary diagnosis and management of other diseases.

MATERIALS AND METHODS

Ethical Approval All animal care and experimental procedures adhered to the ARVO Statement for the Use of Animals in Ophthalmic and Vision Research and received approval from the Institutional Animal Care and Use Committee of Zhongshan Ophthalmic Center, Sun Yat-sen University (Approval number: SYXK [YUE] 2023-0189).

Animals Eight-week-old male type 2 diabetic (BKS-Leprem^{2Cd479}/Gpt; *db*/*db*) mice were obtained from GemPharmatech Co., Ltd. (Nanjing, China). The *db*/*db* mice carry a spontaneous mutation in the leptin receptor, leading to the development of type 2 diabetes[20]. Animals were maintained under specific pathogen-free conditions with a 12-hour light/ dark cycle (8:00 *a.m.*–8:00 *p.m.*), temperature of 23°C±1°C, and humidity of 60%±5%. Following a one-week acclimatization period with free access to standard chow and water, diabetes was confirmed in *db*/*db* mice by measuring blood glucose levels exceeding 16.7 mmol/L for two consecutive days.

To explore the effects on ocular surface dysfunction and MG abnormalities of different dietary patterns in the *db*/*db* model, *db*/*db* mice were allocated into two experimental groups (n=15 per group) based on general and ocular surface health: an *ad libitum* (AL) group with continuous access to food and water, and an IF group subjected to one day of fasting followed by free diet (water continuously available).

Animal Examination A single masked ophthalmologist assessed and photographed eyelid margins using a slit-lamp microscope (SL-D7/DC-3/IMAGEnet, Topcon, Tokyo, Japan) before and after the intervention. Mice were anesthetized *via* intraperitoneal injection of 1% pentobarbital sodium prior to ocular surface examination.

Following euthanasia, entire upper and lower eyelids were excised. MGs were then dissected by carefully removing other tissues, such as overlying skin, muscle, and hair follicles. We aimed to meet the statistical power requirements for different experiments within the limited number of animals permitted by ethical guidelines because of the limited weight of the MGs in mouse model. All samples from different groups were randomly assigned to different experimental subgroups. Four mice per group were randomly selected for Western blot (WB) analysis of their MGs. Five MGs per group underwent transcriptomic analysis, while bilateral glands from six mice per group were analyzed for lipidomics. Remaining MGs were reserved for morphological examination. MG morphology was documented using a stereoscopic zoom microscope (ZEISS SteREO Discovery V8, Jena, Germany), and gland area was quantified using Image J software. Following imaging, selected MGs were processed for paraffin embedding, sagittal/coronal frozen sectioning, or lipidomic/ transcriptomic analyses.

Histology MG tissues underwent fixation in 4% paraformaldehyde (PFA), dehydration through a sucrose gradient (10%, 20%, 30%), and paraffin embedding. Frozen sections (8 μm thick, sagittal and coronal) were prepared and stored at -80°C for LipidTox staining and immunofluorescence. Paraffin-embedded sections (5 μm thick, sagittal) were stored at room temperature for hematoxylin and eosin (HE) staining and immunohistochemistry.

LipidTox Staining MG sections were washed four times in phosphate-buffered saline (PBS), then incubated with high content screening (HCS) LipidTox solution (1:500, H34475; Invitrogen, Grand Island, NY, USA) for 30min at room

temperature to label neutral lipids. Nuclei were counterstained with 4',6-diamidino-2-phenylindole (DAPI; 1 μg/mL; Biofroxx, Germany) for 20min. Images were captured using a confocal laser scanning microscope (ZEISS; LSM 980, Oberkochen, Germany).

Immunohistochemical Staining Paraffin sections were deparaffinized, rehydrated, and subjected to antigen retrieval in 10 mmol/L sodium citrate buffer (80°C, 10min). After cooling, endogenous peroxidase was blocked with 3% H_2O_2, followed by blocking with phosphate-buffered saline with Tween-20 (PBST) containing 10% donkey serum. Sections were incubated overnight with primary rabbit antibodies: 3-hydroxy-3-methylglutaryl-coenzyme a reductase (HMGCR; 1:1000, A16875; Abclonal, Wuhan, China), calcium-sensing receptor (CaSR; 1:100, GB115579; Servicebio, Wuhan, China), calcium channel, voltage-dependent, beta 4 subunit (CACNB4; 1:3000, GB114354; Servicebio, Wuhan, China). After PBS washes, sections were incubated with horseradish peroxidase (HRP)-conjugated secondary antibody (1:200, GB23303; Servicebio, Wuhan, China), counterstained with hematoxylin, and imaged (Tissue FAXS Q+, TissueGnostics, Vienna, Austria).

Immunofluorescence Staining Sagittal and coronal MG sections were permeabilized (0.25% Triton X-100) and blocked [PBS with 3% bovine serum albumin (BSA)]. Primary antibodies were applied overnight at 4°C: Ki67 (1:150, MA5-14520; Invitrogen, CA, USA), p63 (1:100, ab124762; Abcam, Cambridge, MA, USA), Lrig1 (1:100, AF3688; R&D Systems, Minneapolis, MN, USA), cytokeratin 1 (K1; 1:50, ab185628; Abcam), cytokeratin 10 (K10; 1:50, ab76318; Abcam) for coronal sections. Sections were then incubated for 1h in the dark at room temperature with fluorophore-conjugated secondary antibodies: Alexa Fluor 555 donkey anti-rabbit IgG (1:500, ab155062; Abcam), Alexa Fluor 647 donkey anti-goat IgG (1:500, ab150135; Abcam). Nuclei were counterstained with DAPI (20min). Imaging used a confocal laser scanning microscope (ZEISS; LSM 980).

TUNEL Assay Apoptosis in frozen eyelid sections was detected using a TdT-mediated dUTP nick-end labeling (TUNEL) Apoptosis Detection Kit (Vazyme, Nanjing, China) per manufacturer's protocol. Briefly, sections were fixed (4% PFA, 30min), treated with proteinase K (10min), equilibrated in buffer (10min), incubated with TUNEL reaction mixture (37°C, 1h, humidified dark chamber), and counterstained with DAPI. Images were captured by confocal microscopy (ZEISS; LSM 980).

Transmission Electron Microscopy Tissues were fixed overnight in 2.5% glutaraldehyde (4°C), post-fixed in 1% osmium tetroxide, stained with uranyl acetate, and embedded in epoxy resin. Ultrathin sections (100 nm) were cut (Leica EM UC7 microtome, Wetzlar, Germany) and imaged using a Tecnai G2 Spirit transmission electron microscopy [TEM (FEI)].

RNA Sequencing Total RNA was extracted from MGs using TRIzol reagent. mRNA was purified, fragmented (200-300 bp), and used for cDNA synthesis (random hexamers for first strand; buffer, dNTPs, RNase H, DNA polymerase I for second strand). The Illumina Hiseq™ 6000 sequencer generated sequencing data with PE150 reads. Lianchuan Biotechnology Co., Ltd. (Hangzhou, China) performed the transcriptome analysis. Differentially expressed genes (DEGs) were identified using EdgeR (threshold: $|\log_2$ fold change (FC)$| \geq 1$, $P<0.05$). Gene Ontology (GO) and Kyoto Encyclopedia of Genes and Genomes (KEGG) pathway analyses were conducted. Differential expression results were visualized using scatter plots and volcano plots of DEGs, created in R.

Lipidomics Analysis Metabolites were extracted by adding 120 μL precooled extraction buffer (IPA:ACN:H_2O=2:1:1) to 20 μL sample, vortexing (1min), incubating (10min), and storing overnight (at -20°C). After centrifugation (4000 g, 20min, 4°C), supernatants were transferred and stored at -80°C pending liquid chromatography-mass spectrometry (LC-MS) analysis. Pooled quality control (QC) samples were prepared by combining 10 μL of each extraction mixture. Metabolites were detected using a Q-Exactive high-resolution tandem mass spectrometer (Thermo Scientific, USA).

Statistical Analysis (Lipidomics) Statistical analyses in R (version 4.0.0) included hierarchical clustering (pheatmap), and PLS-DA analysis (ropls) with VIP value calculation. Pearson's correlation analysis identified metabolites meeting criteria: $P<0.05$, FC>1.2, and significant VIP values.

Hypergeometric enrichment analysis (KEGG) pathway annotated metabolites. Gene Set Enrichment Analysis (GSEA v4.1.0, MSigDB) evaluated enrichment in KEGG pathways (significance criteria: |NES|>1, NOM P-value <0.05, and FDR Q-value <0.25). A pathway-based metabolite network map was generated.

Protein Extraction and Western Blot The upper MGs of the treated eye of a mouse were combined to create a protein sample. Freshly dissected and minced MGs were immediately homogenized in cold RIPA lysis buffer containing PMSF and phosphatase inhibitors (Sigma-Aldrich). Protein concentration was determined (BCA assay kit, Solarbio, Beijing, China). Proteins (25 μg) were separated on 4%-20% SDS-PAGE gels (Bio-Rad, CA, USA) and transferred to PVDF membranes. Membranes were blocked (3% BSA, 2h), then incubated overnight with primary antibodies: HMGCR (1:1000, A16875; Abclonal), Lrig1 (1:1000, AF3688; R&D Systems), K1 (1:1000, ab185628, Abcam), K10 (1:1000, ab76318, Abcam),

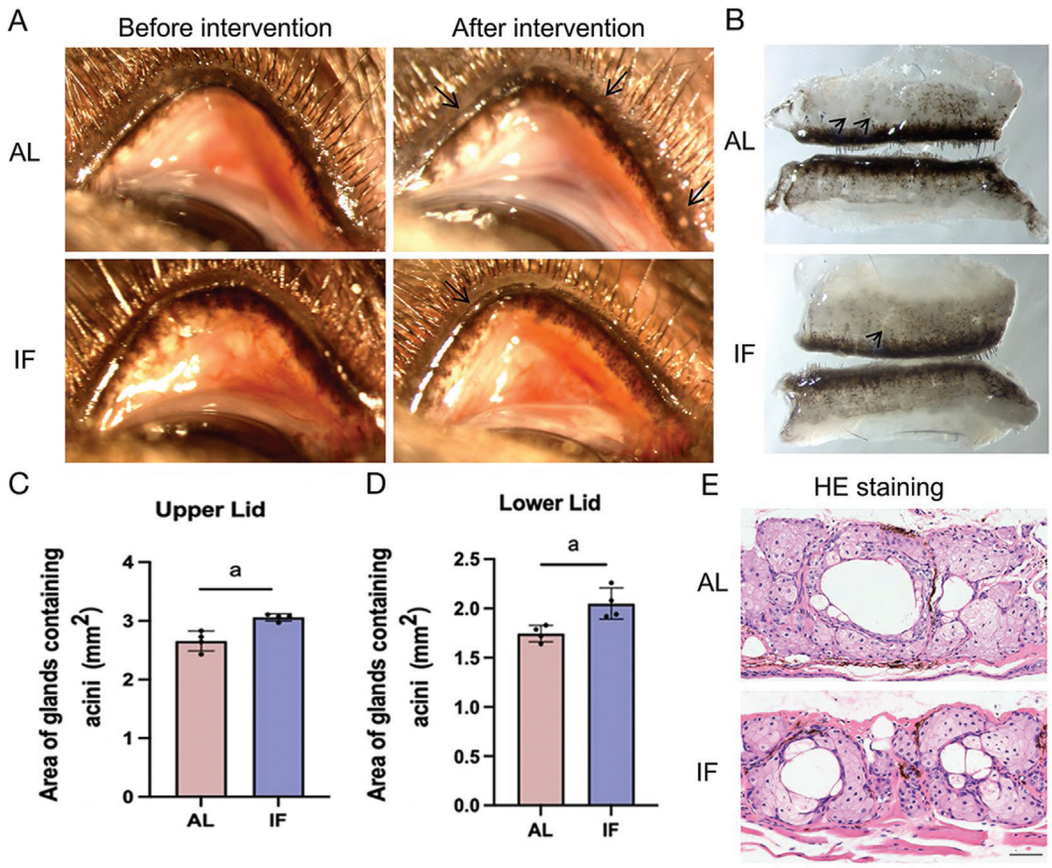

Figure 1 IF relieved diabetes-induced MGD A: Slit-lamp observation of MG openings before and after intervention (black arrows: MG duct obstruction); B: Stereomicroscopic analysis of MG (black arrows: MG atrophy); C: The area of glands containing acini in the upper lids increased in IF-treated mice (*n*=4); D: The area of glands containing acini in the lower lids increased in IF-treated mice (*n*=4); E: HE staining of MG (scale bar: 50 μm). Data are expressed as mean±SD, [a]*P*<0.05. IF: Intermittent fasting; MGD: Meibomian gland dysfunction; MG: Meibomian gland; HE: Hematoxylin and eosin; SD: Standard deviation; AL: *Ad libitum*.

β-actin (1:2000, 4970S, CST, Boston, MA, USA). After washing, membranes were incubated with HRP-conjugated secondary antibodies (goat anti-rabbit IgG, 1:5000, ab6378; donkey anti-goat IgG, 1:5000, ab6885). Signal was detected using enhanced chemiluminescence. Bands were visualized and quantified (Bio-Rad Gel Doc XR, Image Lab 5.1 software).

Image Processing and Statistical Analysis Immunocytochemistry and immunofluorescence data were quantified using Image J. For TUNEL immunofluorescence, the ratio of positive cells to DAPI-stained nuclei in MGs was calculated. LipidTox fluorescence intensity was calculated as integrated density per high-power field area. Three biological replicates were used in immunofluorescence assays, with at least six images per replicate analyzed statistically.

Statistical significance for comparisons between two groups was determined using unpaired two-tailed Student's *t*-tests and one-way analysis of variance (Prism 8, GraphPad Software). Data were presented as mean±standard deviation (SD). Statistical significance was defined as $P<0.05$. Results represent at least three independent biological replicates.

RESULTS

IF Improves Diabetes-Induced MGD To explore the potential induction of MGD pathological alterations under distinct dietary regimens, we initially employed slit lamp biomicroscopy to evaluate characteristic MGD manifestations. Comparative analysis between AL and IF dietary groups demonstrated that IF intervention significantly ameliorated diabetes-induced MG ductal obstruction (Figure 1A). Macroscopic morphological assessments further demonstrated IF-mediated improvements in acinar architecture, including normalization of acinar size distribution (Figure 1B-1D).

IF improved the abnormal expansion of the duct and the aggregation of abnormal cells around the acini compared to AL (Figure 1E).

IF Ameliorates the Proliferation, Apoptosis and Obstruction of MG in Diabetes Mouse IF intervention partially restored proliferative capacity in diabetic MG, the immunofluorescence staining intensity of p63, Ki67 and Lrig1 of MG in the IF group increased partly (Figure 2A-2C). In the meantime, the WB results of p63 and Lrig1 also supported this result (Figure 2D). This series of experiments suggested that

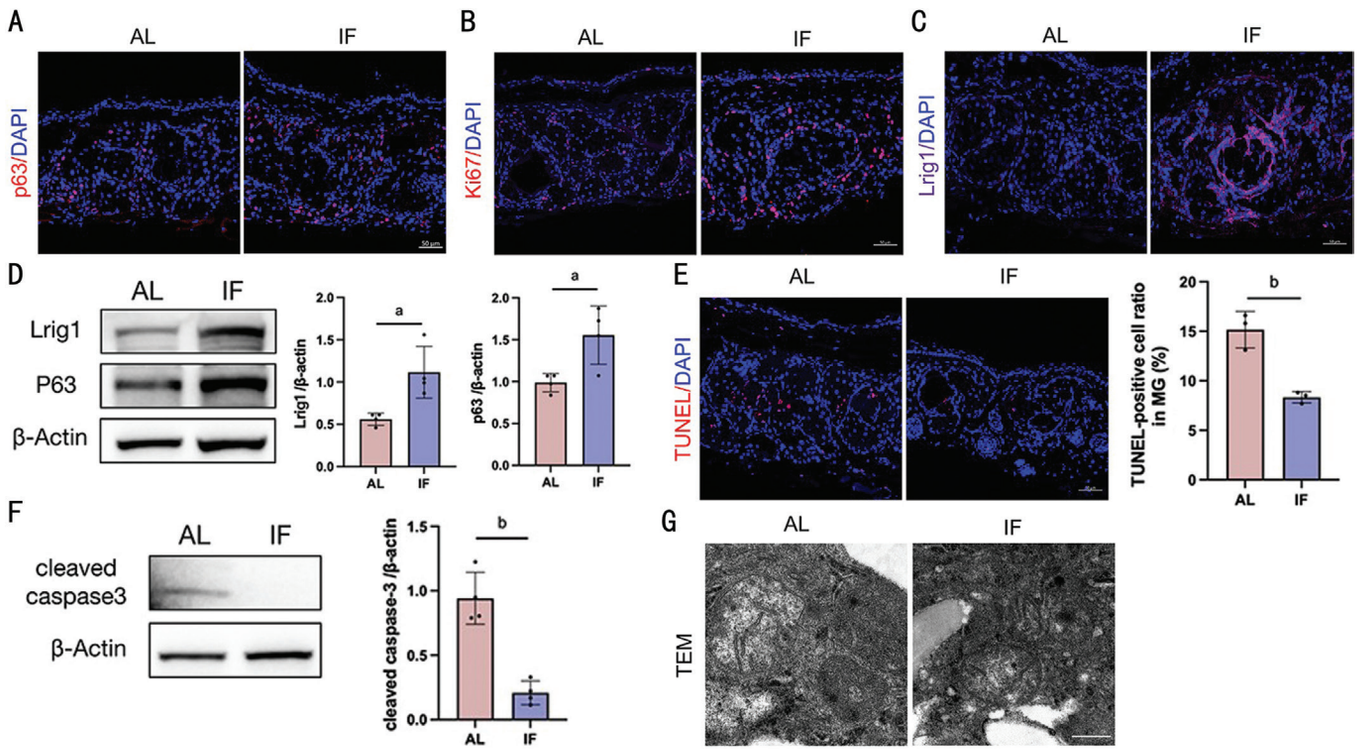

Figure 2 IF rescued abnormal acinar cell proliferation and apoptosis of MG caused by diabetes A: The representative graph of p63 immunofluorescent staining demonstrated positive expression within the basal cells of MG acini (scale bar: 50 μm); B: Ki67 immunofluorescent staining demonstrated positive expression within the basal cells of MG acini (scale bar: 50 μm); C: Lrig1 immunofluorescent staining demonstrated positive expression within the basal cells of MG acini (scale bar: 50 μm); D: WB analysis revealed significantly higher levels of p63 and Lrig1 in MG of the IF group (n=4); E: TUNEL immunofluorescent staining and cell counts decreased in MG of the IF group (scale bar: 50 μm); F: WB analysis revealed lower level of cleaved caspase-3 in MG of the IF group (n=4); G: TEM revealed the mitochondrial morphology in acini cells of MGs in the two different groups (scale bar: 1 μm). Data are expressed as mean±SD, ^{a}P<0.05, ^{b}P<0.01. IF: Intermittent fasting; MG: Meibomian gland; WB: Western blot; TEM: Transmission electron microscopy; TUNEL: Terminal deoxynucleotidyl transferase-mediated dUTP nick end labeling; SD: Standard deviation; AL: *Ad libitum*; DAPI: 4',6-diamidion-2-phenylindole.

IF mediated activation of progenitor cell populations to some extent.

To assess apoptotic cell death, TUNEL staining results showed that few TUNEL-positive cells could be observed in the IF group, the cell death was significantly improved (Figure 2E). Meanwhile, immunohistochemical results showed that IF could downregulate cleaved caspase-3 expression in the acinar cells of MG, WB result and its quantification also hinted cleaved caspase-3 expression decreased in the IF group (Figure 2F). Finally, TEM showed after the IF intervention, the mitochondrial damage, including swelling of the mitochondria, was mitigated notably (Figure 2G). These results indicated that IF was protective against the abnormal death of MG cells caused by diabetes.

Slit-lamp biomicroscopy demonstrated that IF could significantly improve blockage of MG during the intervention. Given the established association between ductal hyperkeratinization and MGD[21], we selected K1 and K10, two biomarkers of keratinized epithelium, to evaluate keratinization. From the immunofluorescence images, we found that the expression of K1 and K10 decreased after IF intervention (Figure 3A). Furthermore, the WB results were also consistent with these immunofluorescence results (Figure 3B, 3C). These data collectively indicated that IF attenuated diabetes-induced ductal hyperkeratinization and also improved the diabetes-induced MGD.

IF Alleviates Lipid Metabolic Disorders We have found that IF could significantly reduce obstruction of diabetic MG. Existing research has established that MG obstruction induces significant alterations in lipid dynamics, manifesting as impaired lipid transport efficiency and subsequent pathological accumulation of lipid droplets. This mechanistic pathway has been shown to disrupt the physiological homeostasis of the ocular surface microenvironment[22]. Next, to study the distribution of lipids in MG, the tissue sections were stained by LipidTox. LipidTox staining and its quantification analysis revealed that IF markedly attenuated pathological lipid deposition in MG (Figure 4A, 4B). TEM analysis demonstrated that in the AL group, substantial lipid accumulation with clump-like aggregates was observed within

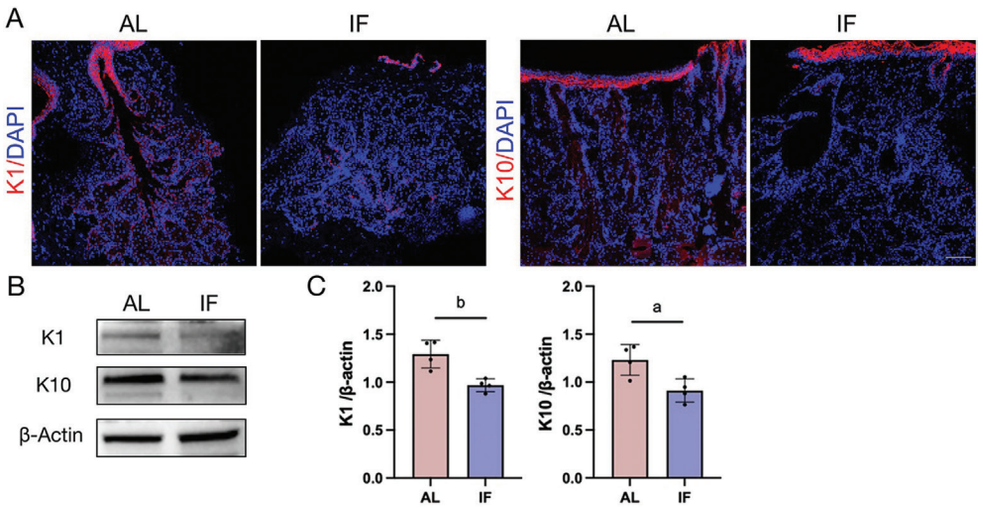

Figure 3 IF ameliorated MG hyperkeratinization The representative graph of K1 and K10 immunofluorescent staining (A; scale bar: 100 μm); Western blot (B) and its quantification (C) revealed significantly reduced levels of K1 and K10 in MG of the IF group (*n*=4). Data are expressed as mean±SD, [a]*P*<0.05, [b]*P*<0.01. IF: Intermittent fasting; MG: Meibomian gland; SD: Standard deviation; AL: *Ad libitum*; DAPI: 4′,6-diamidion-2-phenylindole.

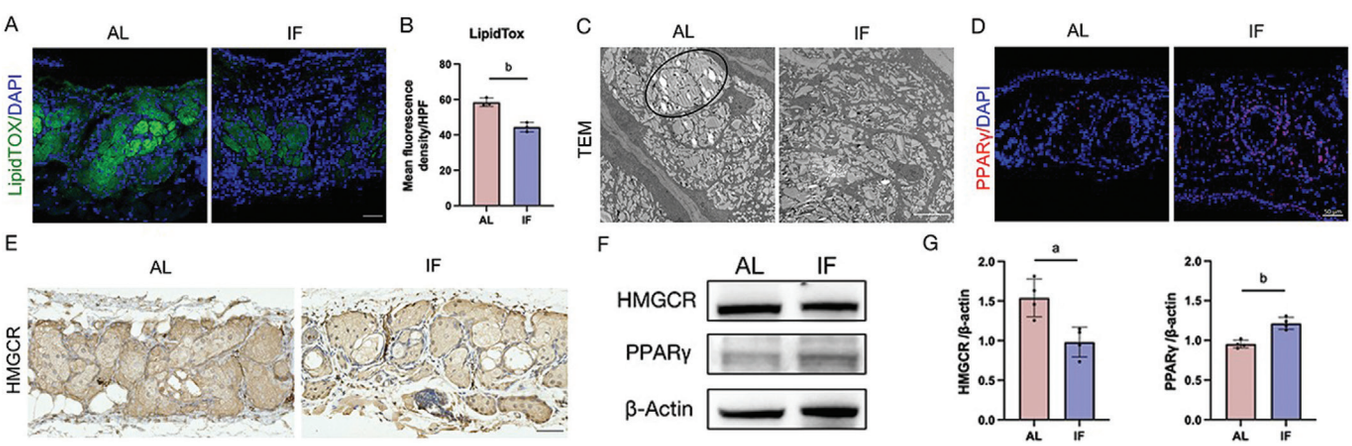

Figure 4 IF rescued diabetes-induced meibum metabolism disorder A: The representative graph of LipidTox Green staining demonstrated lipid accumulation within acini (scale bar: 50 μm); B: LipidTox Green staining showed lower fluorescence intensity in the IF group (*n*=3); C: TEM showed MG acinar cells exhibited excessive lipid accumulation, with lipids fused into aggregates in the AL group (scale bar: 10 μm, black circle: merging of lipids); D: PPARγ immunofluorescent staining demonstrated positive expression within the basal cells of MG acini (scale bar: 50 μm); E: HMGCR immunohistochemical analysis revealed decreased expression in MG after IF intervention (scale bar: 50 μm); F, G: WB and its analysis revealed lower level of HMGCR and higher level of PPARγ in MG of the IF group (*n*=4). Data are expressed as mean±SD, [a]*P*<0.05, [b]*P*<0.01. IF: Intermittent fasting; MG: Meibomian gland; TEM: Transmission electron microscopy; PPARγ: Peroxisome proliferator-activated receptor gamma; HMGCR: 3-hydroxy-3-methylglutaryl-CoA reductase; WB: Western blot; AL: *Ad libitum*; SD: Standard deviation; DAPI: 4′,6-diamidion-2-phenylindole.

MG cell, thereby impeding lipid fluidity and excretion. However, no such significant lipid aggregation was noted in the IF group (Figure 4C).

There was a pathophysiological association between MGD and dyslipidemia, with particular relevance to diabetes-associated metabolic disturbances. Previous studies have demonstrated that chronic hyperglycemia disrupts lipid homeostasis in MG acinar cells, inducing both qualitative alterations in lipid composition and pathological intracellular accumulation[13]. To investigate the potential mechanistic links between metabolic dysregulation and glandular dysfunction, we conducted targeted analyses of critical lipid metabolic regulators: HMGCR, the key enzyme in cholesterol biosynthesis, and PPARγ, a master regulator of lipid metabolism[23]. We found that the HMGCR expression significantly decreased in the IF group, while PPARγ increased (Figure 4D, 4E). This tendency was further confirmed by WB analysis (Figure 4F, 4G). These results indicated that IF could ameliorate lipid metabolism disorder in MG caused by diabetes to some extent.

MGs Lipidome Changes Between AL and IF Groups in Diabetic Mice Through Metabolomic Analysis In order to explore the changes of lipid metabolism in MG after different

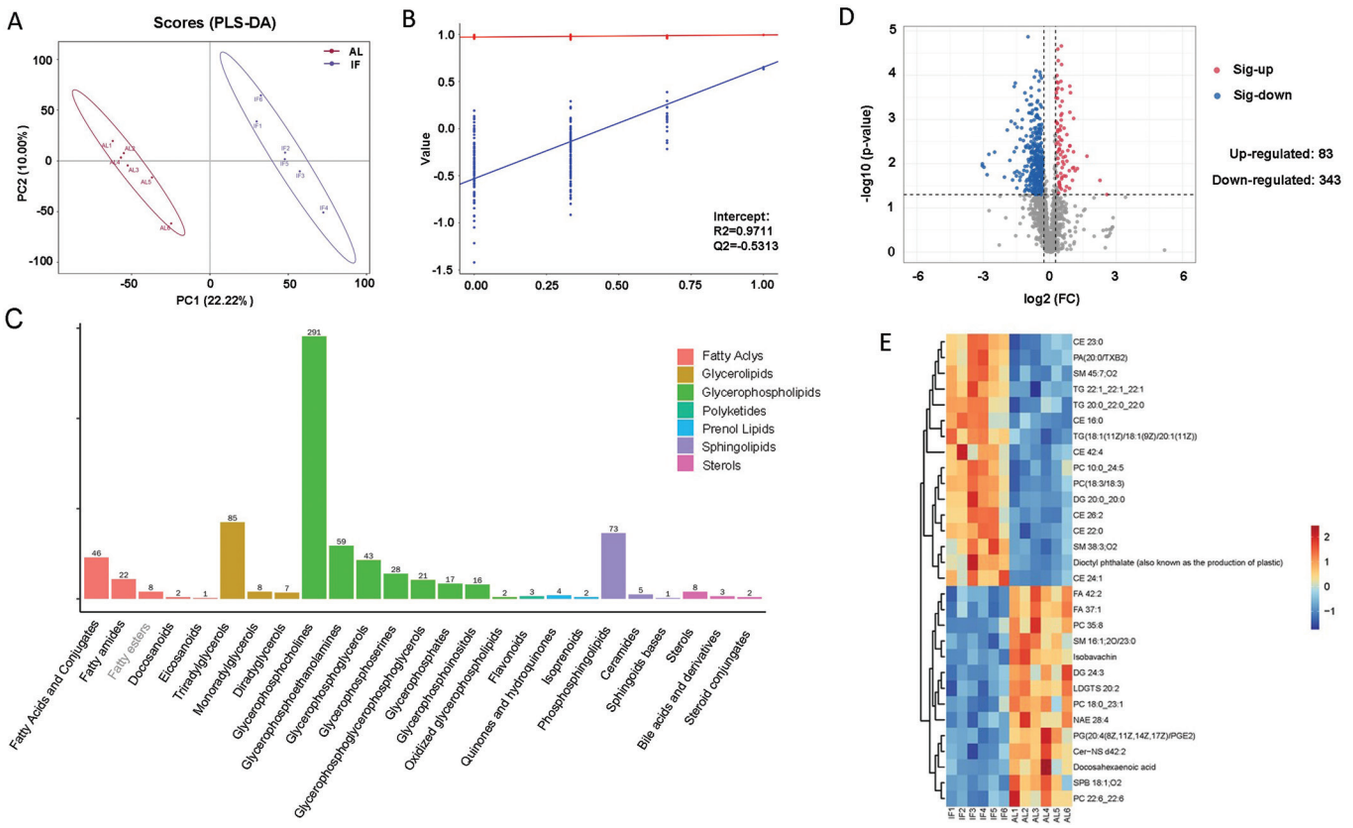

Figure 5 Lipidomic analysis of MGs in the AL and IF groups A: PLS-DA scores plot presenting AL (red) and IF (blue) with significant separation and predictability; B: The PLS-DA model's validation over 200 iterations of permutation testing; C: The identified lipid subclasses and the number of lipid species per lipid subclass; D: Volcano plot of identified lipids including up-regulated and down-regulated lipids in AL and IF groups; E: Heatmap displaying sample clusters (*n*=6) and the top 30 significantly changed lipid species (red and blue-filled lines indicate increased and decreased levels of lipids, respectively); Alteration of sphingolipids and glycerolipids in AL and IF groups. MG: Meibomian gland; IF: Intermittent fasting; AL: *Ad libitum*; PLS-DA: Partial least-squares discriminant analysis.

dietary interventions, we next performed in-depth lipidomic analysis. The results of multivariate statistical analysis through the partial least-squares discriminant analysis (PLS-DA) models were shown in Figure 5. As shown in PLS-DA plot (Figure 5A), values of $Q2>0.5$, indicated that the model was stable and reliable. To assess the quality of the models and check for overfitting, the models were subjected to permutation testing. The intercept values of $R2$ and $Q2$ were 0.97 and -0.53 (Figure 5B). These results indicated that the results had low overfitting risk and high reliability, demonstrating the well performance of this model and showing significant differences between AL and IF groups. Untargeted lipidomics analysis was performed to study the lipidomic profiling in AL and IF groups. According to the LC-MS/ MS spectra, we identified 1898 lipid molecules and quantified them. The results showed that the identified lipids were divided into 25 lipid subclasses, among which the most diverse was glycerophosphocholines (*n*=292), followed by triradylglycerols (*n*=85) and phosphosphingolipids (*n*=73; Figure 5C).

The changes of the detected lipid molecules of MGs in different groups were analyzed and displayed in a volcano graph (Figure 5D, FC>1.5 and $P<0.05$ considered as statistical differences). We found a total of 426 differentially expressed molecules in diabetic MGs of IF group compared with those of AL group, of which 83 were up-regulated and 343 were down-regulated (Figure 5D). The top 30 lipid molecules showing the greatest changes were displayed in the cluster heatmap, and it is notable that different types of the cholesteryl esters decreased in the IF group (Figure 5E).

Key Gene Expression Changes Between AL and IF Groups in Diabetic Mice from Transcriptome Results As shown in Figure 6A and 6B, transcriptome sequencing found 256 DEGs in the MG tissue, including 164 upregulated genes and 92 downregulated genes. Enrichment analysis was conducted to investigate the biological response to IF in the MG tissue, specifically focusing on molecular function, cellular components, and biological processes (Figure 6D). The DEGs were primarily enriched in 25 GO terms (level 2) within the biological process category. In the cellular component category, the DEGs were mainly associated with three GO terms (level 2): membrane, plasm membrane, and cytoplasm. In terms of molecular function, the top two GO terms (level 2)

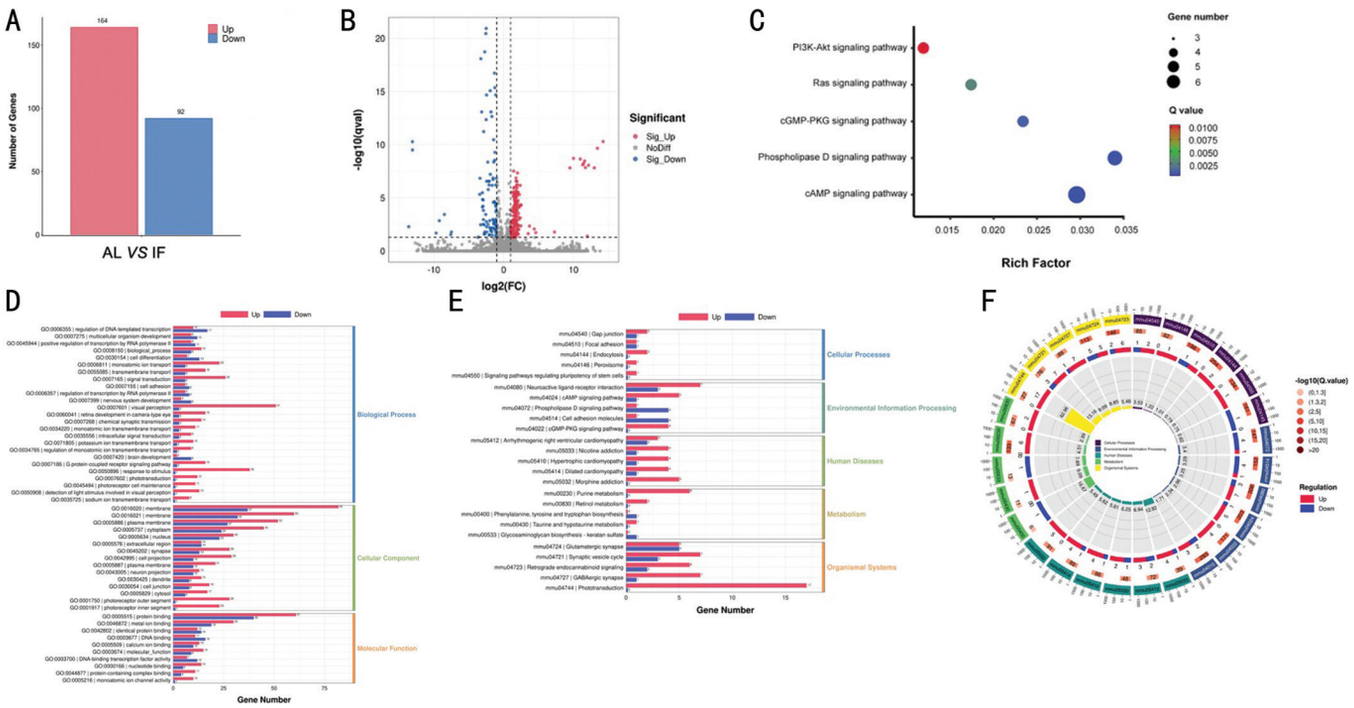

Figure 6 Transcriptomic analysis of MGs in the AL and IF groups A: Number of significantly upregulated and down-regulated genes in different groups; B: Volcano plot of identified genes including up-regulated and down-regulated genes in AL and IF groups; C: Significantly differential KEGG terms related to apoptosis; D: GO enrichment analysis for the MGs between the AL and IF groups; E: KEGG enrichment analysis for the MGs between the AL and IF groups; F: The significantly enriched KEGG pathways. MG: Meibomian gland; IF: Intermittent fasting; AL: *Ad libitum*; KEGG: Kyoto Encyclopedia of Genes and Genomes; GO: Gene Ontology.

were protein binding and metal ion binding.

Furthermore, IF resulted in significant changes in five KEGG terms related to apoptosis (Figure 6C): PI3K-Akt signaling pathway (*P*-adjust<0.001), Ras signaling pathway (*P*-adjust=0.0015), cGMP-PKG signaling pathway (*P*-adjust<0.001), Phospholipase D signaling pathway (*P*-adjust=0.0015), and cGMP signaling pathway (*P*-adjust=0.0015).

As shown in Figure 6E and 6F, 256 DEGs were found to be enriched in 5 kinds of KEGG level 1 and 25 kinds of KEGG level 2. Specifically, IF resulted in significant changes in 28 pathways, including gap junction, phospholipase D signaling pathway, and taurine and hypotaurine metabolism.

Comprehensive Analysis of Lipidomic and Transcriptomic Analysis To further investigate the biological functions and regulatory mechanisms of IF in the MGs of diabetic mouse, we conducted a combined analysis to evaluate the potential association between alteration in transcriptional profiles and lipid profiles. Our results revealed that 54 pathways were commonly enriched in both mRNA and metabolites (Figure 7A). The differential lipid metabolites in the lipid profile were strictly screened by the lipidomic analysis based on *P*-values (*P*<0.05). As shown in Figure 7B and 7C, compared with the AL group, IF group significantly affected 16 lipid metabolites. The most abundantly identified lipid categories were cholesterol sulfate and LysoPA. Additionally, the genes *Cngb1*, *Cnga1*, and *Cacng8* belong to the calcium signaling pathway. Subsequently, we constructed a network diagram to visualize the key targets identified through integrated analysis of transcriptomic and lipidomic datasets. The central nodes representing critical targets within the network were specifically highlighted through visual magnification to emphasize their topological importance and functional relevance in the biological system under investigation. Notably, the network plot demonstrated that calcium signaling pathway was the key pathway among the altered pathways induced by IF (Figure 7D).

From conjoint analysis of lipidomics and transcriptomics, our investigation identified calcium signaling as one of the principal pathways mechanistically involved in mediating MG alterations during dietary intervention. We selected one of the most important genes of this pathway, Calcium sensing receptor (CaSR), for immunohistochemical analysis[24-25]. Figure 7E showed that CaSR was significantly reduced in the IF group, suggesting that IF reduced its expression, thereby inhibiting the regulation of central channels in the calcium signaling pathway, affecting the G protein pathway and calcium ions, which might affect cell death. As a functional role in calcium signaling pathway, CACNB4 may regulate intracellular calcium concentrations by modulating the

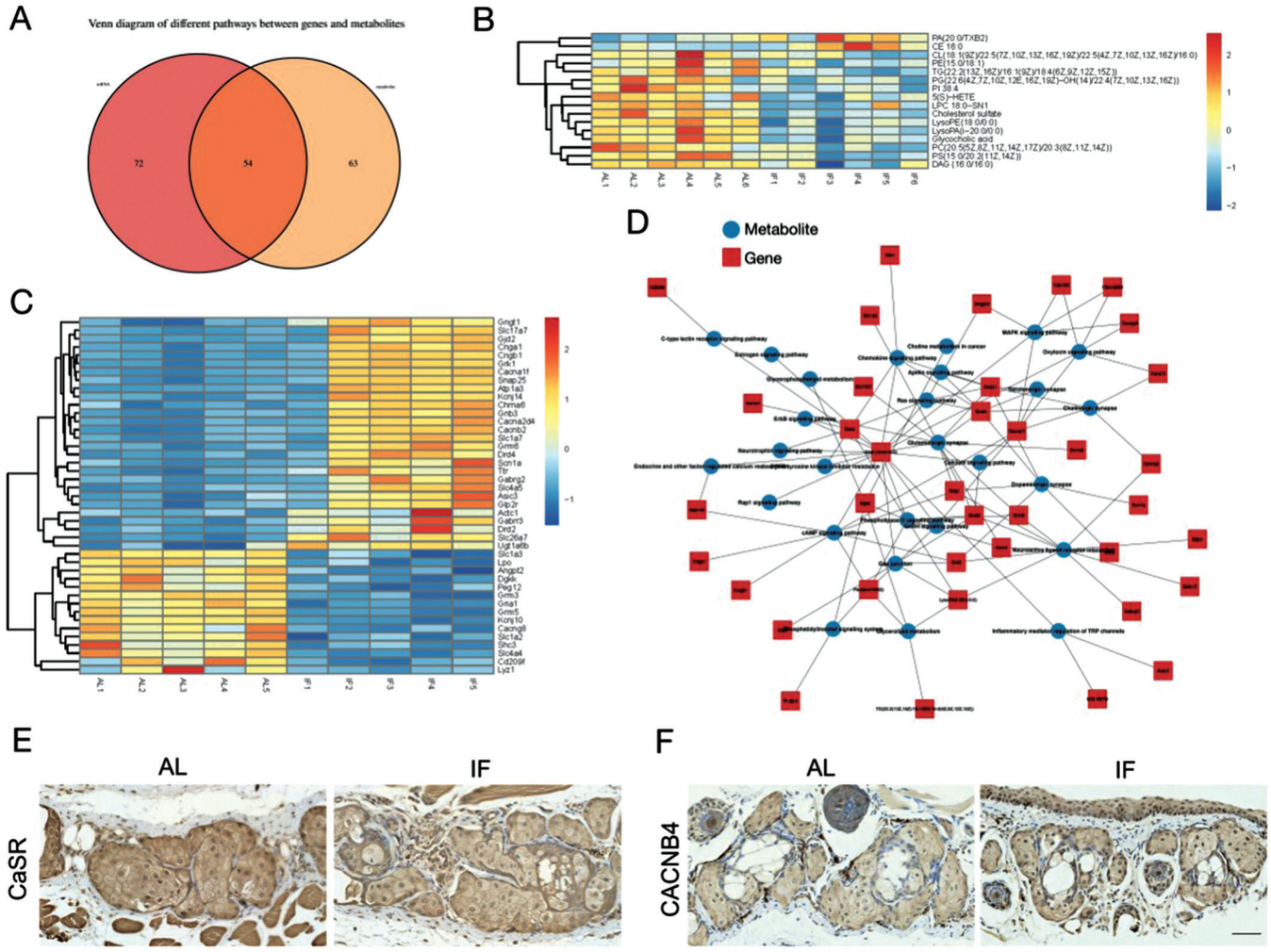

Figure 7 Comprehensive analysis of lipidomic and transcriptomic analysis of MGs in the AL and IF groups A: Venn diagram of different pathways between genes and metabolites in lipidomic and transcriptomic analysis; B: Heatmap of significantly different metabolite clusters; C: Heatmap of significantly different gene clusters; D: KEGG network diagram involved lipidomic and transcriptomic analysis, calcium signaling pathway was identified as the key pathway; E: Representative immunohistochemical staining for CaSR in the two groups (scale bar: 50 μm); F: Representative immunohistochemical staining for CACNB4 in the two groups (scale bar: 50 μm). MG: Meibomian gland; IF: Intermittent fasting; AL: *Ad libitum*; KEGG: Kyoto Encyclopedia of Genes and Genomes; CaSR: Calcium sensing receptor.

gating of calcium, thus regulating cell proliferation and cell cycle progression[26]. It presented stronger staining in the IF group (Figure 7F). This suggested that IF might promote its expression, and the changes of calcium ions are dynamic and regulated by multiple factors.

DISCUSSION

Mounting evidence has shown that diabetes was not only one of the causes of MGD but also could aggravate MGD[27]. Hyperglycemic and hyperlipidemic states could disrupt MG metabolism through aberrant expression of lipid metabolism-related proteins, culminating in pathological lipid accumulation, ductal obstruction, and acinar atrophy[3,23,28]. Particularly, diabetes induces quantitative and qualitative alterations in meibomian lipids, characterized by modified lipid class ratios and compositional changes[29].

Current therapeutic strategies for lipid accumulation-induced MGD remain limited in specificity, though PPARγ agonists have shown preliminary efficacy[30]. Notably, dietary interventions have gained prominence in diabetes management, with IF demonstrating systemic metabolic benefits in obesity and diabetic complications such as diabetic retinopathy[31-33]. However, emerging evidence suggested IF might exert different effects in different tissues, with certain studies documenting adverse outcomes including immune system modulation[34]. However, the precise mechanistic interplay between IF intervention and MG remains to be elucidated. Our study revealed that IF effectively mitigated diabetes-induced abnormal lipid deposition in MGs, reduced apoptotic cell death, and alleviated glandular duct obstruction.

Previous studies have reported that various factors, including diabetic status and high fat diet, could lead to abnormal expression of enzymes related to lipid metabolism in the

MG[3,28,35]. Our findings demonstrated that IF improved the expression of key genes involved in MG lipid metabolism and reduced the abnormal lipid accumulation observed in diabetic MGs. Notably, our comprehensive analysis of lipidomic and transcriptomic analysis revealed for the first time that IF reversed this pathological process by restructuring the lipid metabolic network.

Diabetes could significantly affect the lipid composition of the MG, altering levels of cholesterol esters, ceramide and other contents[29]. Changes in these lipids may mediate the reduced cell proliferation and increase inflammation[36-37]. Our results demonstrated that IF altered the changes in the MG caused by diabetes, primarily focusing on lipid changes such as fatty acids, glycerolipids, and glycerophospholipids. Specifically, IF significantly reduced levels of various components of cholesterol esters.

Diabetes primarily impacts cell proliferation and apoptosis in the MG[38-39]. Transcriptomics analysis in our research suggested that IF improved diabetes-induced MGD mainly through biological processes, cellular structure and function, as well as pathways closely related to the ion transport pathways of MG. KEGG pathway analysis indicated that the effects of IF on diabetic MGs were associated with cell junctions, phospholipase D signaling pathway, ion transport, and various metabolic processes.

Diabetes induces heightened apoptotic susceptibility in MG acinar cells, mechanistically mediated through oxidative stress and autophagy, collectively contributing to glandular atrophy[13,40]. Our investigation demonstrated that IF might show a protective effect by ameliorating diabetes-induced pathological cell death cascades, mechanistically paralleling its cytoprotective efficacy observed in other organ systems[41-43]. Comprehensive analysis of transcriptomic and lipidomic datasets revealed that the central key pathway of the joint analysis was related to ion channels, especially calcium ion channels. The calcium signaling cascades functions as a pleiotropic regulator of cellular homeostasis, transducing extracellular stimuli into intracellular responses through spatiotemporal fluctuations in cytoplasmic Ca^{2+} concentration[44-46]. This mechanism has been described to coordinate diverse cellular processes, including cell cycle progression, programmed death pathways, and secretory vesicle trafficking[47-49]. Intriguingly, calcium signaling cascades in MGs which have been less extensively characterized compared to other secretory tissues. Integrative multi-omics profiling, along with immunohistochemical validation of CaSR and CACNB4, identified calcium signaling as a key mechanism. The beneficial effects of IF on diabetes-induced aberrant cell death may be correlated with activity in this signaling axis.

However, the precise mechanisms through which IF modulated calcium ion channels to influence apoptosis, as well as the specific interactions, remain incompletely elucidated. Furthermore, potential discrepancies in lipid composition and gene expression profiles of MGs between humans and mice still need to be further explored[50]. Also, we did not employ calcium channel regulators to validate their effects on the MGs *in vitro* or *in vivo*. These aspects will be further elucidated in future research. Additionally, we used male mice to maintain consistency with previous studies on diabetes-related MGD[36] and to minimize variability in the early-stage diabetic phenotype. However, this is also a limitation of our study, and we will address sex differences in future research.

In conclusion, our work delineated the network between lipid, calcium signaling and diabetes-induced MGD pathogenesis.

ACKNOWLEDGEMENTS

Foundations: Supported by the National Natural Science Foundation of China (No.82371021; No.82070922); the Natural Science Foundation of Guangdong Province (No.2023A1515012336; No.2023A1515030079; No.2023A1515010091); the Guangzhou City Plan Project (No.2023A03J0172).

Conflicts of Interest: Wang WH, None; **Wu HY,** None; **Xue JW,** None; **Qian XB,** None; **Li J,** None; **Lin XY,** None; **Yang BY,** None; **Wang W,** None; **Liang LY,** None.

REFERENCES

1 Zhu XM, Xu MG, Portal C, *et al*. Identification of Meibomian gland stem cell populations and mechanisms of aging. *Nat Commun* 2025;16:1663.

2 Green-Church KB, Butovich I, Willcox M, *et al*. The international workshop on meibomian gland dysfunction: report of the subcommittee on tear film lipids and lipid–protein interactions in health and disease. *Invest Ophthalmol Vis Sci* 2011;52(4):1979.

3 Bu JH, Zhang MJ, Wu Y, *et al*. High-fat diet induces inflammation of meibomian gland. *Invest Ophthalmol Vis Sci* 2021;62(10):13.

4 Saha RK, Mahmud Chowdhury AM, Na KS, *et al*. Automated quantification of meibomian gland dropout in infrared meibography using deep learning. *Ocul Surf* 2022;26:283-294.

5 Sheppard JD, Nichols KK. Dry eye disease associated with meibomian gland dysfunction: focus on tear film characteristics and the therapeutic landscape. *Ophthalmol Ther* 2023;12(3):1397-1418.

6 Suzuki T, Kitazawa K, Cho Y, *et al*. Alteration in meibum lipid composition and subjective symptoms due to aging and meibomian gland dysfunction. *Ocul Surf* 2022;26:310-317.

7 Kim WJ, Ahn YJ, Kim MH, *et al*. Lipid layer thickness decrease due to meibomian gland dysfunction leads to tear film instability and reflex tear secretion. *Ann Med* 2022;54(1):893-899.

8 Qazi Y, Kheirkhah A, Blackie C, *et al*. Clinically relevant immune-cellular metrics of inflammation in meibomian gland dysfunction. *Invest Ophthalmol Vis Sci* 2018;59(15):6111.

9 Shaw JE, Sicree RA, Zimmet PZ. Global estimates of the prevalence of diabetes for 2010 and 2030. *Diabetes Res Clin Pract* 2010;87(1):4-14.

10 Sandra Johanna GP, Antonio LA, Andrés GS. Correlation between type 2 diabetes, dry eye and Meibomian glands dysfunction. *J Optom* 2019;12(4):256-262.

11 Hao YR, Wu BG, Feng J, *et al*. Relationship between type 2 diabetes mellitus and changes of the lid margin, meibomian gland and tear film in dry eye patients: a cross-sectional study. *Int Ophthalmol* 2025;45(1):261.

12 Yu T. Morphological and cytological changes of meibomian glands in patients with type 2 diabetes mellitus. *Int J Ophthalmol* 2019;12(9):1415-1419.

13 Ding J, Liu Y, Sullivan DA. Effects of insulin and high glucose on human meibomian gland epithelial cells. *Invest Ophthalmol Vis Sci* 2015;56(13):7814.

14 Treasure J, Duarte TA, Schmidt U. Eating disorders. *Lancet* 2020;395(10227):899-911.

15 Hall KD. Energy compensation and metabolic adaptation: "The Biggest Loser" study reinterpreted. *Obesity* 2022;30(1):11-13.

16 Clinthorne JF, Beli E, Duriancik DM, *et al*. NK cell maturation and function in C57BL/6 mice are altered by caloric restriction. *J Immunol* 2013;190(2):712-722.

17 Varady KA, Cienfuegos S, Ezpeleta M, *et al*. Clinical application of intermittent fasting for weight loss: progress and future directions. *Nat Rev Endocrinol* 2022;18(5):309-321.

18 Ezpeleta M, Gabel K, Cienfuegos S, *et al*. Effect of alternate day fasting combined with aerobic exercise on non-alcoholic fatty liver disease: a randomized controlled trial. *Cell Metab* 2023;35(1):56-70.e3.

19 Ezzati A, Rosenkranz SK, Phelan J, *et al*. The effects of isocaloric intermittent fasting vs daily caloric restriction on weight loss and metabolic risk factors for noncommunicable chronic diseases: a systematic review of randomized controlled or comparative trials. *J Acad Nutr Diet* 2023;123(2):318-329.e1.

20 Couturier A, Calissi C, Cracowski JL, *et al*. Mouse models of diabetes-related ulcers: a systematic review and network meta-analysis. *eBioMedicine* 2023;98:104856.

21 Nichols KK, Foulks GN, Bron AJ, *et al*. The international workshop on meibomian gland dysfunction: executive summary. *Invest Ophthalmol Vis Sci* 2011;52(4):1922.

22 Suzuki T. Inflamed obstructive meibomian gland dysfunction causes ocular surface inflammation. *Invest Ophthalmol Vis Sci* 2018;59(14):DES94.

23 Guo YL, Zhang HJ, Zhao ZY, *et al*. Hyperglycemia induces meibomian gland dysfunction. *Invest Ophthalmol Vis Sci* 2022;63(1):30.

24 Conigrave AD, Ward DT. Calcium-sensing receptor (CaSR): Pharmacological properties and signaling pathways. *Best Pract Res Clin Endocrinol Metab* 2013;27(3):315-331.

25 Adam S, Maas SL, Huchzermeier R, *et al*. The calcium-sensing-receptor (CaSR) in adipocytes contributes to sex-differences in the susceptibility to high fat diet induced obesity and atherosclerosis. *EBioMedicine* 2024;107:105293.

26 Rima M, Daghsni M, Lopez A, *et al*. Down-regulation of the Wnt/β-catenin signaling pathway by Cacnb4. *Mol Biol Cell* 2017;28(25):3699-3708.

27 Mohamed-Noriega K, González-Arocha CS, Morales-Wong F, *et al*. Meibomian gland dysfunction and dropout in diabetic patients with non-proliferative diabetic retinopathy. *Bioengineering (Basel)* 2024;11(9):907.

28 Silva-Viguera MC, Pérez-Barea A, Bautista-Llamas MJ. Tear film layers and meibomian gland assessment in patients with type 1 diabetes mellitus using a noninvasive ocular surface analyzer: a cross-sectional case–control study. *Graefes Arch Clin Exp Ophthalmol* 2023;261(5):1483-1492.

29 Wang HF, Zhou QJ, Wan LQ, *et al*. Lipidomic analysis of meibomian glands from type-1 diabetes mouse model and preliminary studies of potential mechanism. *Exp Eye Res* 2021;210:108710.

30 Yu F, Zhao X, Wang Q, *et al*. Photothermal-responsive soluble microneedle patches for meibomian gland dysfunction therapy. *Adv Sci* 2025:e2413962.

31 Obermayer A, Tripolt NJ, Pferschy PN, *et al*. Efficacy and safety of intermittent fasting in people with insulin-treated type 2 diabetes (interfast-2)-a randomized controlled trial. *Diabetes Care* 2023;46(2):463-468.

32 Teong XT, Liu K, Vincent AD, *et al*. Intermittent fasting plus early time-restricted eating versus calorie restriction and standard care in adults at risk of type 2 diabetes: a randomized controlled trial. *Nat Med* 2023;29(4):963-972.

33 Beli E, Yan YQ, Moldovan L, *et al*. Restructuring of the gut microbiome by intermittent fasting prevents retinopathy and prolongs survival in *db*/*db* mice. *Diabetes* 2018;67(9):1867-1879.

34 Janssen H, Kahles F, Liu D, *et al*. Monocytes re-enter the bone marrow during fasting and alter the host response to infection. *Immunity* 2023;56(4):783-796.

35 Zou S, Liu JM, Si HL, *et al*. High-fat intake reshapes the circadian transcriptome profile and metabolism in murine meibomian glands. *Front Nutr* 2023;10:1146916.

36 Osae EA, Bullock T, Chintapalati M, *et al*. Obese mice with dyslipidemia exhibit meibomian gland hypertrophy and alterations in meibum composition and aqueous tear production. *Int J Mol Sci* 2020;21(22):8772.

37 Butovich IA. Lipidomics of human Meibomian gland secretions: chemistry, biophysics, and physiological role of meibomian lipids. *Prog Lipid Res* 2011;50(3):278-301.

38 Yang Q, Liu LH, Li J, *et al*. Evaluation of meibomian gland dysfunction in type 2 diabetes with dry eye disease: a non-randomized controlled trial. *BMC Ophthalmol* 2023;23(1):44.

39 Wu HP, Fang X, Luo SR, *et al*. Meibomian glands and tear film findings in type 2 diabetic patients: a cross-sectional study. *Front Med* 2022;9:762493.

40 Wang J, Chen SP, Zhao XX, *et al*. Effect of PPARγ on oxidative stress in diabetes-related dry eye. *Exp Eye Res* 2023;231:109498.

41 Choi JH, Cho YJ, Kim HJ, *et al*. Effect of carbohydrate-restricted diets and intermittent fasting on obesity, type 2 diabetes mellitus, and hypertension management: consensus statement of the Korean Society for the Study of Obesity, Korean Diabetes Association, and Korean Society of Hypertension. *Clin Hypertens* 2022;28(1):26.

42 Liu ZG, Dai XS, Zhang HB, *et al*. Gut microbiota mediates intermittent-fasting alleviation of diabetes-induced cognitive impairment. *Nat Commun* 2020;11:855.

43 Hammer SS, Vieira CP, McFarland D, *et al*. Fasting and fasting-mimicking treatment activate SIRT1/LXRα and alleviate diabetes-induced systemic and microvascular dysfunction. *Diabetologia* 2021;64(7):1674-1689.

44 Rinne A, Pluteanu F. Ca^{2+} signaling in cardiovascular fibroblasts. *Biomolecules* 2024;14(11):1365.

45 Goyani S, Shukla S, Jadiya P, *et al*. Calcium signaling in mitochondrial intermembrane space. *Biochem Soc Trans* 2024;52(5):2215-2229.

46 Crul T, Maléth J. Endoplasmic reticulum-plasma membrane contact sites as an organizing principle for compartmentalized calcium and cAMP signaling. *Int J Mol Sci* 2021;22(9):4703.

47 Bedi O, Sapra V, Kumar M, *et al*. Newer mitochondrial dynamics and their role of calcium signalling in liver regeneration. *Mitochondrion* 2024;79:101969.

48 Bacsa B, Hopl V, Derler I. Synthetic biology meets Ca^{2+} release-activated Ca^{2+} channel-dependent immunomodulation. *Cells* 2024;13(6):468.

49 Sukumaran P, Nascimento Da Conceicao V, Sun YY, *et al*. Calcium signaling regulates autophagy and apoptosis. *Cells* 2021;10(8):2125.

50 Osae EA, Steven P, Redfern R, *et al*. Dyslipidemia and meibomian gland dysfunction: utility of lipidomics and experimental prospects with a diet-induced obesity mouse model. *Int J Mol Sci* 2019;20(14):3505.